

# Chapter 18 Spline Element I—Analysis of High-Rise Building Structures

Yu-Qiu Long

Department of Civil Engineering, School of Civil Engineering,  
Tsinghua University, Beijing, 100084, China

Zhong Fan

China Architecture Design and Research Group, Beijing, 100044, China

**Abstract** This chapter discusses the spline element method, which is the result obtained by the combination of the spline function and the finite element method. Firstly, the characteristics of the spline functions and spline elements are given. Then, the beam and membrane element models constructed by the spline functions are presented. Finally, some applications of these spline elements in the analysis of the shear wall and tube structures are illustrated.

**Keywords** finite element, spline function, spline element, high-rise building structure.

## 18.1 Introduction

In the finite element method, a structure will be divided by the elements with piecewise interpolation functions.

The most commonly used piecewise polynomials are Lagrangian interpolations, Hermitian interpolations, spline functions, and so on. Compared with other piecewise polynomials, the spline functions have many advantages. For example, they contain fewer undetermined coefficients; possess high-order continuity; and exhibit high approximate performance. Therefore, the spline function method is increasingly important for various numerical analyses<sup>[1-4]</sup>.

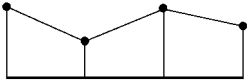

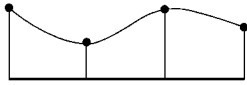
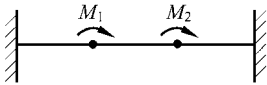
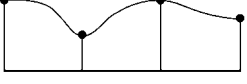

$n$ -order spline function is a piecewise  $n$ -order polynomial with  $C_{n-1}$ -continuity. The configurations and corresponding mechanics models of linear, quadratic and cubic spline functions are given in Table 18.1.

There are two application patterns of the spline functions in structure analyses. One is the global interpolation scheme, such as the spline variation method and

the spline weighted residual method. The other is the piecewise interpolation scheme, which is called the spline finite element method<sup>[5-9]</sup>. The common advantage of these two patterns is that more accurate and smoother solutions can be obtained with fewer degrees of freedom. But, the former is only suitable for domains with regular shapes, while the latter can be conveniently used for structures with complicated geometry.

The spline finite element method is the topic discussed in this and the next chapters.

**Table 18.1** Configurations of spline functions and their mechanics models

	Configurations	Mechanics models
Linear spline	 <p><math>C_0</math>-continuity piecewise fold line</p>	 <p>Displacement curve of a suspended-cable subjected to concentrated loads</p>
Quadratic spline	 <p><math>C_1</math>-continuity piecewise parabolic curve</p>	 <p>Displacement curve of a beam subjected to concentrated couples</p>
Cubic spline	 <p><math>C_2</math>-continuity piecewise cubic parabolic curve</p>	 <p>Displacement curve of a beam subjected to concentrated forces</p>

## 18.2 Spline Beam Elements

Two low-order spline beam elements are introduced in this section. And, the spline thick beam elements considering shear deformation will be given in Sect. 19.2.

### 18.2.1 Quadratic Spline Beam Element (4 Degrees of Freedom)

A quadratic spline beam element is shown in Fig. 18.1. Its element nodal displacement vector contains 4 degrees of freedom:

$$\mathbf{q}^e = [w_1 \quad \theta_1 \quad w_2 \quad \theta_2]^T$$

The element is divided into two segments 13 and 32. Assume that the deflection  $w(x)$  is quadratic polynomial within each segment:

$$w(x) = \begin{cases} c_1 + c_2\xi + c_3\xi^2 & \left( 0 \leq \xi \leq \frac{1}{2} \right) \\ c_4 + c_5\xi + c_6\xi^2 & \left( \frac{1}{2} \leq \xi \leq 1 \right) \end{cases} \quad (18-1)$$

$$\xi = \frac{x}{a}, \theta = \frac{dw}{dx}$$

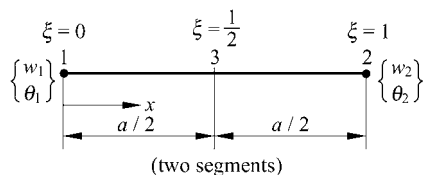


Figure 18.1 Quadratic spline beam element

in which 6 unknown coefficients  $c_1, \dots, c_6$  can be determined by the following 6 conditions

$$\left. \begin{aligned} w|_{\xi=0} = w_1, \quad w|_{\xi=1} = w_2, \quad w|_{\xi=\frac{1}{2}-0} = w|_{\xi=\frac{1}{2}+0} \\ \frac{dw}{dx}|_{\xi=0} = \theta_1, \quad \frac{dw}{dx}|_{\xi=1} = \theta_2, \quad \frac{dw}{dx}|_{\xi=\frac{1}{2}-0} = \frac{dw}{dx}|_{\xi=\frac{1}{2}+0} \end{aligned} \right\} \quad (18-2)$$

Therefore,  $w(x)$  can be expressed in terms of 4 shape functions as follows

$$w(x) = N_1^{(0)}(x)w_1 + N_1^{(1)}(x)\theta_1 + N_2^{(0)}(x)w_2 + N_2^{(1)}(x)\theta_2 \quad (18-3)$$

where the shape functions are all quadratic spline functions

$$\left. \begin{aligned} N_1^{(0)}(x) &= \begin{cases} 1 - 2\xi^2 & \left( 0 \leq \xi \leq \frac{1}{2} \right) \\ 2(1 - \xi)^2 & \left( \frac{1}{2} \leq \xi \leq 1 \right) \end{cases} \\ N_1^{(1)}(x) &= \begin{cases} \frac{a}{2}\xi(2 - 3\xi) & \left( 0 \leq \xi \leq \frac{1}{2} \right) \\ \frac{a}{2}(1 - \xi)^2 & \left( \frac{1}{2} \leq \xi \leq 1 \right) \end{cases} \\ N_2^{(0)}(x) &= 1 - N_1^{(0)}(x) \\ N_2^{(1)}(x) &= -N_1^{(1)}(a - x) \end{aligned} \right\} \quad (18-4)$$

Finally, the element stiffness matrix can be obtained

$$K^e = \begin{bmatrix} 16 & 8a & -16 & 8a \\ & 5a^2 & -8a & 3a^2 \\ \text{Sym.} & & 16 & -8a \\ & & & 5a^2 \end{bmatrix} \quad (18-5)$$

### 18.2.2 Cubic Spline Beam Element (6 Degrees of Freedom)

A cubic spline beam element is shown in Fig. 18.2. Its element nodal displacement vector contains 6 degrees of freedom:

$$q^e = [w_1 \quad w_1' \quad w_1'' \quad w_2 \quad w_2' \quad w_2'']^T$$

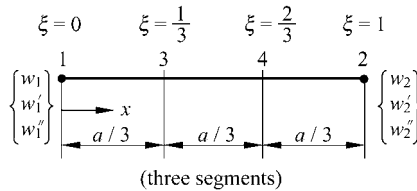


Figure 18.2 Cubic spline beam element

The element is divided into three segments 13, 34 and 42. Assume that the deflection  $w(x)$  is cubic polynomial within each segment. It contains 12 unknown coefficients, which can be determined by the boundary conditions at end nodes 1 and 2, and continuous conditions at virtual nodes 3 and 4 of deflection and its first and second order derivatives. Hence,  $w(x)$  can be expressed in terms of the 6 shape functions as follows:

$$w(x) = N_1^{(0)}(x)w_1 + N_1^{(1)}(x)w_1' + N_1^{(2)}(x)w_1'' + N_2^{(0)}(x)w_2 + N_2^{(1)}(x)w_2' + N_2^{(2)}(x)w_2'' \quad (18-6)$$

in which the shape functions are all cubic spline functions

$$N_1^{(0)}(x) = \begin{cases} 1 - \frac{9}{2}\xi^3 & \left( 0 \leq \xi \leq \frac{1}{3} \right) \\ \frac{1}{6}[5 - 3(3\xi - 1) - 3(3\xi - 1)^2 + 2(3\xi - 1)^3] & \left( \frac{1}{3} \leq \xi \leq \frac{2}{3} \right) \\ \frac{9}{2}(1 - \xi)^3 & \left( \frac{2}{3} \leq \xi \leq 1 \right) \end{cases}$$

$$\left. \begin{aligned}
 N_1^{(1)}(x) &= \begin{cases} a\xi(1-3\xi^2) & \left(0 \leq \xi \leq \frac{1}{3}\right) \\
 \frac{a}{18}[4-6(3\xi-1)^2+3(3\xi-1)^3] & \left(\frac{1}{3} \leq \xi \leq \frac{2}{3}\right) \\
 \frac{3}{2}a(1-\xi)^3 & \left(\frac{2}{3} \leq \xi \leq 1\right) \end{cases} \\
 N_1^{(2)}(x) &= \begin{cases} \frac{a^2}{12}\xi^2(6-11\xi) & \left(0 \leq \xi \leq \frac{1}{3}\right) \\
 \frac{a^2}{324}[7+3(3\xi-1)-15(3\xi-1)^2+7(3\xi-1)^3] & \left(\frac{1}{3} \leq \xi \leq \frac{2}{3}\right) \\
 \frac{a^2}{6}(1-\xi)^3 & \left(\frac{2}{3} \leq \xi \leq 1\right) \end{cases} \\
 N_2^{(0)}(x) &= 1 - N_1^{(0)}(x), \quad N_2^{(1)}(x) = -N_1^{(1)}(a-x), \quad N_2^{(2)}(x) = N_1^{(2)}(a-x)
 \end{aligned} \right\} \quad (18-7)$$

Finally, the element stiffness matrix can be obtained

$$\mathbf{K}^e = \frac{EI}{4a^3} \begin{bmatrix} 108 & 54a & 5a^2 & -108 & 54a & -5a^2 \\ & 32a^2 & 3a^3 & -54a & 22a^2 & -2a^3 \\ & & \frac{2}{3}a^4 & -5a^2 & 2a^3 & -\frac{1}{6}a^4 \\ & & & 108 & -54a & 5a^2 \\ \text{Sym.} & & & & 32a^2 & -3a^3 \\ & & & & & \frac{2}{3}a^4 \end{bmatrix} \quad (18-8)$$

### 18.2.3 Numerical Examples

**Example 18.1** A simply-supported beam (span length is  $L$ ) is subjected to uniformly distributed load  $q$ . The flexural rigidity of the beam is  $EI$ . The results and errors of the central deflection and moment by the quadratic and cubic spline elements are listed in Tables 18.2 and 18.3.

**Table 18.2** Central deflection  $w_c / \left(\frac{qL^4}{16EI}\right)$

Number of elements (1/2 beam)	1	2	3	4
Quadratic spline element	0.1979 (5%)	0.2057 (1%)	0.2077 (0.3%)	0.2080 (0.1%)
Cubic spline element	0.2083 (0%)			
Analytical solution	0.2083			

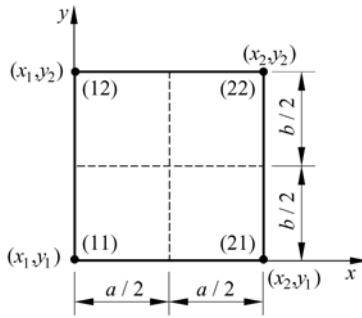
**Table 18.3** Central moment  $M_c / \left( \frac{qL^2}{8} \right)$

Number of elements (1/2 beam)	1	2
Cubic spline element	1.0186 (2%)	1.0046 (0.5%)
Analytical solution	1.0000	

### 18.3 Spline Plane Membrane Elements

The spline plane membrane element is introduced as follows. Assume that the shape of the element is rectangle, and bi-quadratic spline functions are used for interpolation<sup>[10]</sup>.

As shown in Fig. 18.3, a rectangular element is equally divided into 4 sub-regions. And, the coordinates of node  $ij$  ( $i, j = 1, 2$ ) are  $(x_i, y_j)$ .



**Figure 18.3** Rectangular element (4 sub-regions)

There are 8 degrees of freedom at each node  $ij$

$$\mathbf{q}_{ij} = [u_{ij}^{(00)} \quad u_{ij}^{(10)} \quad u_{ij}^{(01)} \quad u_{ij}^{(11)} \quad \vdots \quad v_{ij}^{(00)} \quad v_{ij}^{(10)} \quad v_{ij}^{(01)} \quad v_{ij}^{(11)}]^T \quad (18-9)$$

where

$$\left. \begin{aligned} u_{ij}^{(00)} &= u|_{(x_i, y_j)}, & u_{ij}^{(10)} &= \frac{\partial u}{\partial x} \Big|_{(x_i, y_j)} \\ u_{ij}^{(01)} &= \frac{\partial u}{\partial y} \Big|_{(x_i, y_j)}, & u_{ij}^{(11)} &= \frac{\partial^2 u}{\partial x \partial y} \Big|_{(x_i, y_j)} \end{aligned} \right\} \quad (18-10)$$

Thus, each element has 32 degrees of freedom

$$\mathbf{q}^e = [\mathbf{q}_{11}^T \quad \mathbf{q}_{21}^T \quad \mathbf{q}_{22}^T \quad \mathbf{q}_{12}^T]^T \quad (18-11)$$

The element displacement fields  $u$  and  $v$  can be expressed in terms of the nodal displacements as follows:

$$\begin{Bmatrix} u \\ v \end{Bmatrix} = \sum_{i=1}^2 \sum_{j=1}^2 N_{ij} \mathbf{q}_{ij} \tag{18-12}$$

in which the shape functions are all bi-quadratic spline functions

$$N_{ij} = \begin{bmatrix} N_{ij}^{(00)} & N_{ij}^{(10)} & N_{ij}^{(01)} & N_{ij}^{(11)} & 0 & 0 & 0 & 0 \\ 0 & 0 & 0 & 0 & N_{ij}^{(00)} & N_{ij}^{(10)} & N_{ij}^{(01)} & N_{ij}^{(11)} \end{bmatrix} \tag{18-13}$$

$$N_{ij}^{(kl)}(x, y) = N_i^{(k)}(x)N_j^{(l)}(y) \quad (i, j = 1, 2; \quad k, l = 0, 1) \tag{18-14}$$

$N_i^{(k)}(x)$  are the shape functions of the quadratic spline beam element defined in Eq. (18-4), and  $N_j^{(l)}(y)$  can be defined similarly.

After the determination of the shape functions, the element stiffness matrix can then be obtained by the conventional procedure. This element is denoted as R-OQQ.

**Example 18.2** A simply-supported beam subjected to uniformly distributed load is divided by 6 R-OQQ elements (as shown in Fig. 18.4). The results and comparison of stress  $\sigma_x(0, y)$  by the present element and analytical solution are listed in Table 18.4.

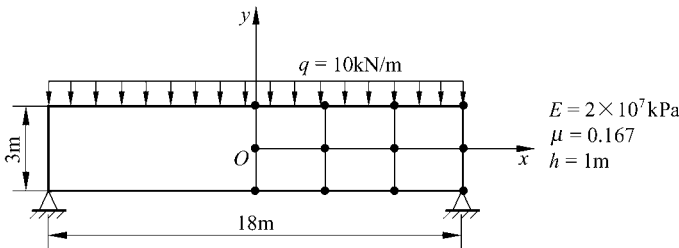


Figure 18.4 A simply-supported beam and mesh division

Table 18.4 Results of stress  $\sigma_x(0, y)$

$y(\text{m})$	1.5	1.0	0.5	0	-0.5	-1.0	-1.5
Present element	-273.4	-180.4	-89.8	-0.6	89.6	181.0	273.1
Analytical	-272.0	-179.5	-89.2	0.0	89.2	179.5	272.0

Details about the spline sectorial and triangular elements can be referred to reference [10].

## 18.4 Analysis of Shear Wall Structures by Spline Elements

Shear wall is one of the important structures popularly used in high-rise buildings.

Ever since finite strip method was proposed by Cheung<sup>[11]</sup> for structure analysis, it has been broadly used in computations of high-rise building structures. And, the longitudinal interpolation functions of strip elements also obtain continuous improvements. However, the common characteristic of this kind of method is that the interpolation procedure must be carried out in the whole strip domain, which is only suitable for the structures with regular shapes. Troubles and difficulties often happen when irregular opening hole and boundary shape exist (Fig. 18.5).

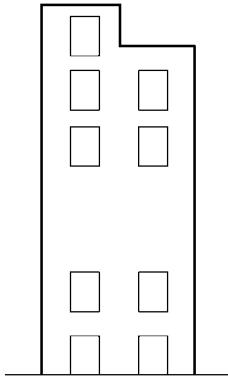


Figure 18.5 Shear wall with opening

Girijavallaham<sup>[12]</sup> used conventional triangular and rectangular elements to analyze the coupled shear wall structures, but the density of the mesh is quite high. Recently, the continuity assumption of structure has been widely accepted. So, in the analysis of structures, the discrete connecting beams can be replaced by the equivalent orthotropic plate, which greatly reduces the number of elements. Chan and Cheung<sup>[13]</sup> proposed a high-order rectangular element, in which the interpolation polynomials of the element transverse and longitudinal displacements are linear and quintic, respectively. Only a few of such elements are enough for the analysis of the whole structure. However, in general, the numerical instability may occur for high-order polynomial approximation.

In this section, a spline element TB-mn which can be broadly used for the analysis of high-rise building structures will be introduced. The displacement components of this spline element are interpolated locally within an element by using the spline function. Then, according to the characteristics of the high-rise building structures, the orders of spline functions for transverse and longitudinal interpolations are selected properly, so that more accurate results can be obtained



by low-order spline functions and fewer degrees of freedom. Since such spline interpolation is performed only within a local element, just as the conventional displacement-based element, this spline element can easily deal with various structure forms with irregular opening holes and boundary shapes.

### 18.4.1 Element TB-mn for the Analysis of High-Rise Building Structures<sup>[8-14]</sup>

For a plane stress rectangular element for the analysis of high-rise building structures (Fig. 18.6), piecewise spline Hermitian interpolation is used for the transverse displacement  $u$  and longitudinal displacement  $v$  of the element

$$\begin{Bmatrix} u \\ v \end{Bmatrix} = \sum_{i=1}^2 \sum_{j=1}^2 \sum_{\alpha=0}^{m-1} \sum_{\beta=0}^{n-1} (N_{mn})_{ij}^{\alpha\beta}(x, y) \begin{Bmatrix} u_{ij}^{\alpha\beta} \\ v_{ij}^{\alpha\beta} \end{Bmatrix} \quad (18-15)$$

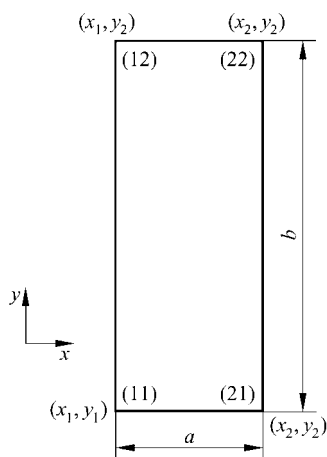


Figure 18.6 Rectangular element

in which  $m$  and  $n$  are the orders of spline functions;  $u_{ij}^{\alpha\beta}$  and  $v_{ij}^{\alpha\beta}$  are the values of displacements or their derivatives at element nodes  $ij$  ( $i, j = 1, 2$ )

$$\begin{Bmatrix} u_{ij}^{\alpha\beta} \\ v_{ij}^{\alpha\beta} \end{Bmatrix} = \left. \frac{\partial^\alpha}{\partial x^\alpha} \frac{\partial^\beta}{\partial y^\beta} \begin{Bmatrix} u(x, y) \\ v(x, y) \end{Bmatrix} \right|_{x=x_i, y=y_j} \quad (18-16)$$

The element shape function  $(N_{mn})_{ij}^{\alpha\beta}(x, y)$  is composed of two piecewise spline interpolation functions

$$(N_{mn})_{ij}^{\alpha\beta} = (N_m)_i^\alpha(x) (N_n)_j^\beta(y) \quad (18-17)$$

**Advanced Finite Element Method in Structural Engineering**

where  $(N_m)_i^\alpha(x)$  and  $(N_n)_j^\beta(y)$  are  $m$  and  $n$  order spline Hermitian interpolation function, respectively; the expressions of  $(N_m)_i^\alpha(x)$  or  $(N_n)_j^\beta(y)$  are as follows:

(1) Linear spline interpolation functions ( $m = 1$ )

$$(N_1)_1^0(x) = 1 - \frac{x+h}{2h} \quad (x \in [-h, h])$$

$$(N_1)_2^0(x) = 1 - (N_1)_1^0(x)$$

(2) Quadratic spline interpolation functions ( $m = 2$ )

$$(N_2)_1^0(x) = \begin{cases} 1 - \frac{(x+2h)^2}{8h^2} & (x \in [-2h, 0]) \\ \frac{(x-2h)^2}{8h^2} & (x \in [0, 2h]) \end{cases}$$

$$(N_2)_1^1(x) = \begin{cases} (x+2h) - \frac{3(x+2h)^2}{8h} & (x \in [-2h, 0]) \\ \frac{(x-2h)^2}{8h} & (x \in [0, 2h]) \end{cases}$$

$$(N_2)_2^0(x) = 1 - (N_2)_1^0(x), \quad (N_2)_2^1(x) = -(N_2)_1^1(-x)$$

(3) Cubic spline interpolation functions ( $m = 3$ )

$$(N_3)_1^0(x) = \begin{cases} 1 - \frac{(x+3h)^3}{48h^3} & (x \in [-3h, -h]) \\ \frac{5}{6} - \frac{x+h}{4h} - \frac{(x+h)^2}{8h^2} + \frac{(x+h)^3}{24h^3} & (x \in [-h, h]) \\ -\frac{(x-3h)^3}{48h^3} & (x \in [h, 3h]) \end{cases}$$

$$(N_3)_1^1(x) = \begin{cases} (x+3h) - \frac{(x+3h)^3}{12h^2} & (x \in [-3h, -h]) \\ \frac{4h}{3} - \frac{(x+h)^2}{2h} + \frac{(x+h)^3}{8h^2} & (x \in [-h, h]) \\ -\frac{(x-3h)^3}{24h^2} & (x \in [h, 3h]) \end{cases}$$

$$(N_3)_1^2(x) = \begin{cases} \frac{(x+3h)^2}{2} - \frac{11(x+3h)^3}{72h} & (x \in [-3h, -h]) \\ \frac{7h^2}{9} + \frac{(x+h)h}{6} - \frac{5(x+h)^2}{12} + \frac{7(x+h)^3}{72h} & (x \in [-h, h]) \\ -\frac{(x-3h)^3}{36h} & (x \in [h, 3h]) \end{cases}$$

$$(N_3)_2^0(x) = 1 - (N_3)_1^0(x)$$

$$(N_3)_2^1(x) = -(N_3)_1^1(-x)$$

$$(N_3)_2^2(x) = (N_3)_1^2(-x)$$

In the above expressions, we have  $h = \frac{a}{2m}$ . And, the interpolation procedure is performed within the range  $\left[-\frac{a}{2}, \frac{a}{2}\right]$  (Fig. 18.6).

Similar to the conventional displacement-based element, the displacement interpolation mode of the spline element can also be written in matrix forms

$$\begin{Bmatrix} u \\ v \end{Bmatrix} = N_{mn} \mathbf{q} \quad (18-18)$$

In the analysis of the high-rise building structures, the longitudinal dimensions of the elements are usually much larger than their transverse dimensions. So  $m \leq n$  is taken when the piecewise interpolation in an element is considered. The spline element constructed by such interpolation mode is called as TB-mn element. When  $m = 1, n = 1$ , the element TB-mn will degenerate to be the ordinary bi-linear plane stress rectangular element.

### 18.4.2 Analysis of Shear Wall Structures by the Element TB-mn

Here, the static and dynamic analyses of the shear wall structures are performed by using the element TB-mn, and several typical examples are given.

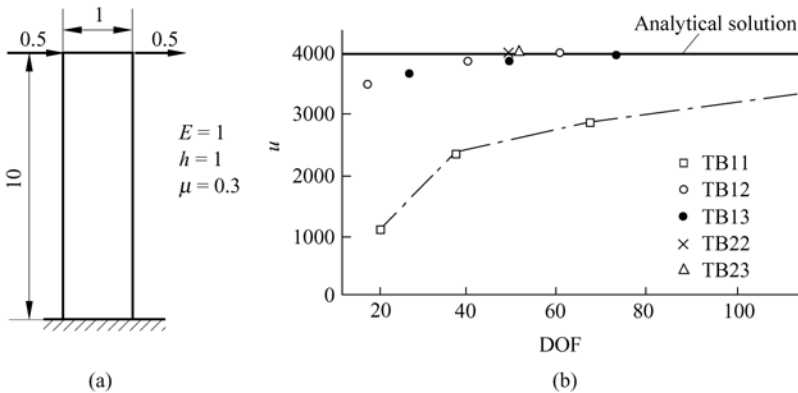
For a shear wall with only small opening, the element TB-mn can be used like the usual rectangular element; for a coupled shear wall structure, the wall limbs can be analyzed directly by the element TB-mn; and the connecting beams are equivalently looked upon as orthotropic continuous grids according to the continuity assumption of the structure. The equivalent elastic and shear modulus of the continuous grids are

$$\left. \begin{aligned} \bar{E}_x &= \frac{d}{h} E \\ \bar{E}_y &= 0 \\ \bar{G} &= \frac{d}{h} \frac{E}{(l/d)^2 + 2.4} \end{aligned} \right\} \quad (18-19)$$

in which  $l$  and  $d$  are the span of the connecting beam and height of beam section, respectively;  $h$  is the storey height of the structure.

**Example 18.3** Tip displacement of a vertical cantilever beam subjected to horizontal load.

In order to test the performance of the element TB-mn, the tip displacement of a vertical cantilever beam subjected to horizontal force is calculated in this example. Geometries and material properties are given in Fig. 18.7(a). The variations of results of tip displacement with total degrees of freedom are plotted in Fig. 18.7(b). Obviously, the convergence speed of the spline element is much faster than that of the usual rectangular element (TB-11). The results obtained from the element TB-mn by the same mesh are listed in Table 18.5. It can be seen that, when only one element is used, the elements TB-22 and TB-23 already reach good accuracy; even the element TB-12, which has only a few nodal degrees of freedom, can improve the precision greatly.



**Figure 18.7** Analysis of shear wall structure by element TB-mn

**Table 18.5** The tip displacement  $u$  of a cantilever beam subjected to horizontal force

Element type	TB-11	TB-12	TB-13	TB-22	TB-23
Nodal degrees of freedom	2	4	6	8	12
Mesh division	1 × 1	102	3452	3649	3724
	1 × 4	1149	3861	3699	4050
Analytical solution	4031				

**Example 18.4** Vibration analysis of a cantilever beam.

Dimensions of the cantilever beam are:  $h \times b = 1.0\text{cm} \times 0.5\text{cm}$ ,  $l = 10\text{cm}$ . Material properties:  $E = 2.1 \times 10^5\text{MPa}$ ,  $\mu = 0.3$ , and mass density  $\rho = 7.8\text{g/cm}^3$ . The results of the natural frequency of the cantilever are listed in Table 18.6.

**Table 18.6** Natural frequencies of a cantilever beam ( $10^3\text{rad/s}$ )

Frequency		First-order			Second-order		
Element type		TB-11	TB-12	TB-13	TB-11	TB-12	TB-13
Mesh division	1 × 1		5.778	5.397		48.93	32.81
	1 × 2		5.450	5.336		34.21	32.58
	1 × 4	9.637	5.337		61.62	32.67	
	1 × 8	6.750			41.21		
	1 × 40	5.532			32.97		

**Example 18.5** Displacement of a coupled shear wall subjected to horizontal load.

In this example, an 11-storey coupled shear wall structure (Fig. 18.8) is calculated by the element TB-mn (Fig. 18.8). The geometrical and physical parameters are as follows:

$$H = 132\text{ft}^*, \quad W = 18\text{ft}, \quad l = 7\text{ft}, \quad d = 2\text{ft}$$

$$h = 12\text{ft}, \quad E = 0.4 \times 10^5\text{kip/ft}^2, \quad \mu = 0.2, \quad t = 1.0\text{ft}$$

For comparison, the usual rectangular element (TB-11) and spline element are both employed. In order to obtain enough precision, the mesh divided by the usual rectangular elements (contains 572 elements) is quite dense. When the computation is performed by the element TB-mn, a continuity treatment must be used for the connecting beams. The lateral displacement curves of the coupled shear wall are plotted in Fig. 18.8(b). It can be seen that satisfactory results can be obtained by quite sparse mesh when the element TB-mn is used.

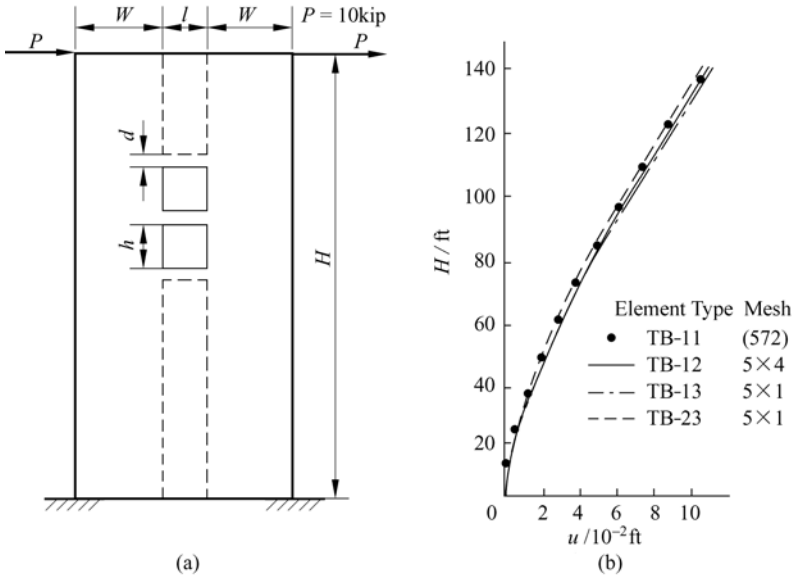
**Example 18.6** Analysis of the shear wall with local stagger holes at the bottom.

A 6-storey shear wall with local stagger holes at the bottom is shown in Fig. 18.9. Young’s modulus  $E = 3.0 \times 10^4\text{MPa}$ , Poisson’s ratio  $\mu = 1/3$ , thickness of the wall is 25cm. The vertical load  $q = 100\text{kN/m}$ , and horizontal load and other parameters are given in Table 18.7.

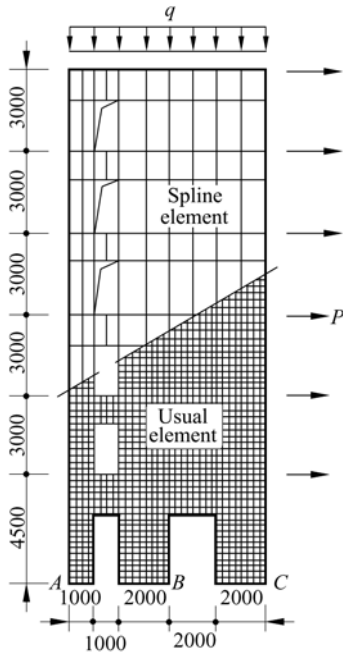
For comparison, the results obtained by the usual element and spline element methods are both given. The mesh divided by the usual model, which contains 2192 elements, is quite dense, while only 104 spline elements TB-13 are utilized.

---

\* ft—feet; kip—kilopound. For comparison with results in related references, units of British Imperial system are used here.



**Figure 18.8** Coupled shear wall structure  
 (a) Structural geometry; (b) Load-displacement curves



**Figure 18.9** Shear wall with local stagger holes at bottom (unit: mm)

From Tables 18.7 and 18.8, it can be seen that, the results of the horizontal displacements of the wall obtained by these two schemes are in good agreement with each other; and, among the computational results of the internal forces at the bottom wall limb, the solutions for the axis forces obtained by the two schemes are in good agreement while the moment solutions have a few differences, however, obvious discrepancies exist in shear force solutions.

**Table 18.7** Parameters and horizontal displacements of a shear wall with stagger holes at the bottom

Storey No.		1	2	3	4	5	6
Storey height (m)		4.500	3.000	3.000	3.000	3.000	3.000
Height of connecting beam (m)		1.500	1.000	1.000	1.000	1.000	1.000
Horizontal force $P_i$ (kN)		36.7	61.2	85.7	110.1	134.6	191.0
Horizontal displacement (mm)	Usual element	0.6446	1.015	1.454	1.890	2.227	2.667
	Spline element	0.6633	1.090	1.577	2.048	2.464	2.875

**Table 18.8** Results of internal forces at bottom wall limb

Wall limb No.		<i>A</i>	<i>B</i>	<i>C</i>
Moment $M$ (kN · m)	Usual element	45.0	499.0	617.5
	Spline element	60.0	396.8	688.4
Axial force $N$ (kN)	Usual element	1040	3161	3803
	Spline element	775	2946	4248
Shear force (kN)	Usual element	6.4	252.8	365.1
	Spline element	22.8	104.7	489.2

## 18.5 Analysis of Frame-Tube Structures by Spline Elements

Frame-tube structure or tube structure, which possesses high spatial stiffness and can perform well in earthquake-resistance, is an ideal structural system for the high-rise and super high-rise buildings. To date, great developments have been achieved in the computational theories of the frame-tube structures. Coull and Subedi<sup>[15]</sup> proposed an equivalent plane frame method in which the frame-tube structure in a 3D space is simplified as a plane frame, so that the computation cost can be greatly reduced. According to the characteristic of “shear lag” in a rectangular frame-tube structure, Coull and Bose<sup>[16,17]</sup> established the corresponding differential equations based on the minimum complementary energy principle. This method is simple, and its accuracy can meet the requirements of design. By assuming that the distribution of the longitudinal stresses along tube section is

piecewise linear, Long et al.<sup>[18]</sup> also established the fundamental equations based on the complementary energy principle. This method can produce high precision solutions for internal forces, and can be used for the computation of the tube structures with arbitrary polygonal section.

The following basic assumptions for the tube structures are employed:

(1) For the floor slab, the in-plane stiffness is infinite rigid, and the out-of-plane stiffness is zero;

(2) The bending stresses at the wall panel of the tube structure are ignored.

For the tube structure with a polygonal section, the whole structure is composed of several wall panels. When we analyze each of these wall panels, local coordinates  $\bar{x}, \bar{y}$  will be firstly employed. Under this local coordinate system, the element stiffness matrix  $\bar{K}^e$  and equivalent nodal load vector  $\bar{p}^e$  of the spline element TB-mn can be obtained. When we analyze the whole tube structure, global coordinates  $x, y, z$  will be used. By the coordinate transformation formulae,  $\bar{K}^e$  and  $\bar{p}^e$ , which are established in the local coordinate system, can be transformed into and assembled in the global coordinate system. The procedure is as follows. The transformation between the local and global coordinate systems is shown in Fig. 18.10.

### 18.5.1 Piecewise Spline Hermitian Interpolation

According to the basic assumptions, the horizontal displacements at the same height of the tube should be the same. Therefore, the horizontal displacement  $\bar{u}$  is interpolated only along the longitudinal direction; but the vertical displacement  $\bar{v}$  is still interpolated by the spline functions along two directions.

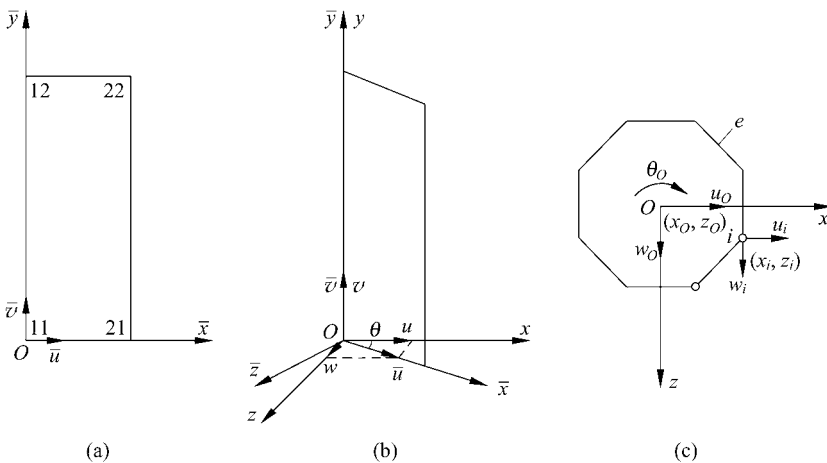


Figure 18.10 Local and global coordinates

(a) Local coordinates; (b) Global coordinates; (c) Coordinate transformation



$$\bar{u} = \sum_{j=1}^2 \sum_{\beta=0}^{n-1} N_{nj}^{\beta}(\bar{y}) \bar{u}_j^{\beta} \quad (18-20)$$

$$\bar{v} = \sum_{i=1}^2 \sum_{j=1}^2 \sum_{\alpha=0}^{m-1} \sum_{\beta=0}^{n-1} N_{mij}^{\alpha\beta}(\bar{x}, \bar{y}) \bar{v}_{ij}^{\alpha\beta} \quad (18-21)$$

In the above equations,  $\bar{u}_j^{\beta}$  and  $\bar{v}_{ij}^{\alpha\beta}$  are the nodal values of displacements or their derivatives in the local coordinate system  $O\bar{x}\bar{y}$  (Fig. 18.10(a)):

$$\bar{u}_j^{\beta} = \frac{\partial^{\beta}}{\partial \bar{y}^{\beta}} \bar{u}(\bar{y}) \Big|_{\bar{y}=\bar{y}_j} \quad (18-22)$$

$$\bar{v}_{ij}^{\alpha\beta} = \frac{\partial^{\alpha}}{\partial \bar{x}^{\alpha}} \frac{\partial^{\beta}}{\partial \bar{y}^{\beta}} \bar{v}(\bar{x}, \bar{y}) \Big|_{\bar{x}=\bar{x}_i, \bar{y}=\bar{y}_j} \quad (18-23)$$

### 18.5.2 Coordinate Transformation

The spline interpolations in the local coordinate system have already been finished above. Here they will be transformed into the global coordinate system (Fig. 18.10(b)). The transformations of the displacement components  $\bar{u}$  and  $\bar{v}$  in the local coordinate system and  $u, v$  and  $w$  in the global coordinate system are

$$\begin{Bmatrix} u \\ v \\ w \end{Bmatrix} = \begin{bmatrix} \cos \theta & 0 \\ 0 & 1 \\ \sin \theta & 0 \end{bmatrix} \begin{Bmatrix} \bar{u} \\ \bar{v} \end{Bmatrix} \quad (18-24)$$

From this equation, the element stiffness matrix  $\bar{\mathbf{K}}^e$  and load vector  $\bar{\mathbf{p}}^e$  can be transformed into the global coordinate system

$$\mathbf{K}^e = \mathbf{T} \bar{\mathbf{K}}^e \mathbf{T}^T, \quad \mathbf{p}^e = \mathbf{T} \bar{\mathbf{p}}^e \quad (18-25)$$

in which  $\mathbf{T}$  is the coordinate transformation matrix

$$\mathbf{T} = \begin{bmatrix} \mathbf{I}_{d_1 \times d_1} \cos \theta & \mathbf{0} \\ \mathbf{0} & \mathbf{I}_{d_1 \times d_1} \\ \mathbf{I}_{d_1 \times d_1} \sin \theta & \mathbf{0} \end{bmatrix} \quad (18-26)$$

$\mathbf{I}$  is the identity matrix;  $d_1 = 2n, d_2 = 4mn$ .

Due to the constraint effect of the floor slab, on any section of the tube, the horizontal displacements ( $u_i, w_i$ ) at node  $i$  ( $i$  is the transverse node number of element  $e, i = 1, 2$ ) can be expressed in terms of the horizontal displacements and angular displacement ( $u_0, w_0, \theta_0$ ) at a reference point on the same section

(Fig. 18.10(c)):

$$\begin{Bmatrix} u_i \\ w_i \end{Bmatrix} = \begin{bmatrix} 1 & 0 & -(z_i - z_0) \\ 0 & 1 & x_i - x_0 \end{bmatrix} \begin{Bmatrix} u_0 \\ w_0 \\ \theta_0 \end{Bmatrix}$$

Thus, at any height of the tube, there are only three horizontal displacements. Here, the global stiffness matrix and load vector of the tube structure can be written as

$$K = \sum_e HT\bar{K}^e T^T H^T \tag{18-27}$$

$$P = \sum_e HT\bar{p}^e \tag{18-28}$$

In the above equations,  $H$  is the transverse constraint matrix

$$H = \begin{bmatrix} I_{d_1 \times d_1} & \mathbf{0} & \mathbf{0} \\ \mathbf{0} & I_{d_2 \times d_2} & \mathbf{0} \\ \mathbf{0} & \mathbf{0} & I_{d_1 \times d_1} \\ A_{d_1 \times d_1} & \mathbf{0} & B_{d_1 \times d_1} \end{bmatrix} \tag{18-29}$$

where  $A$  and  $B$  are the transformation matrices of the nodal displacements ( $u_i, w_i$ ) ( $i = 1, 2$ ) and rotation  $\theta_0$  at the reference point

$$A = \begin{bmatrix} a_1 I_{n \times n} & \mathbf{0} \\ \mathbf{0} & a_2 I_{n \times n} \end{bmatrix}, \quad B = \begin{bmatrix} b_1 I_{n \times n} & \mathbf{0} \\ \mathbf{0} & b_2 I_{n \times n} \end{bmatrix}$$

$$a_i = -(z_i - z_0), \quad b_i = x_i - x_0 \quad (i = 1, 2) \tag{18-30}$$

Some numerical examples of the tube structures with rectangular and polygonal sections are given as follows.

**Example 18.7** Computation of internal forces and displacements of a tube structure with a rectangular section subjected to horizontal load (Fig. 18.11(a),(b)).

The tube structure with a rectangular section is shown in Fig. 18.11(b).

Geometric parameters:  $b/c = 1, H/b = 2, 4, 10, h = \text{constant}$ ; Physical parameters:  $E = \text{constant}, \mu = 0.3$ .

In this example, the tube structure with a rectangular section is analyzed by the elements TB-12 and TB-13. Due to symmetry, only a quarter of the structure is computed. The results of the displacements and internal forces are listed in Tables 18.9 and 18.10. From Table 18.9, it can be seen that the convergence of displacements by the element TB-mn is very good. Since the spline interpolation orders of the element along two directions are selected rationally, the convergence speed of the displacements is faster with the increase of  $H/b$ . The

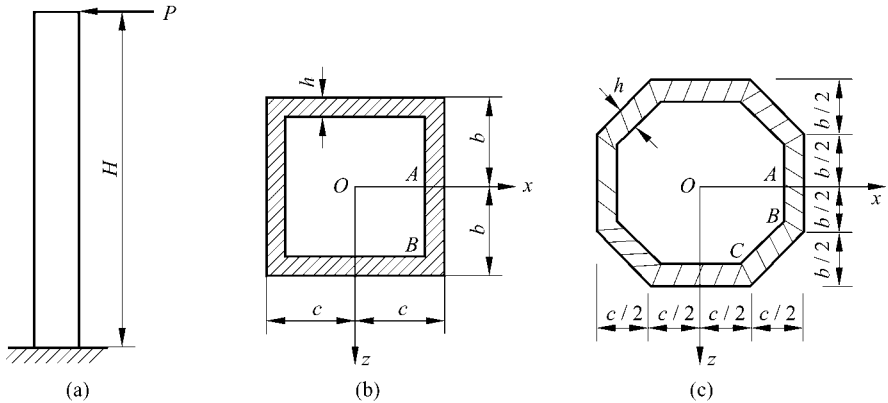


Figure 18.11 Rectangular and polygonal tube structures

Table 18.9 The tip displacement  $u/u_b$  ( $u_b = \frac{PH^3}{3EI}$ ) of a tube structure with rectangular section subjected to horizontal concentrated load

Element type		TB-12			TB-13		
$H/b$		2	4	10	2	4	10
Mesh	1 × 1	3.757	1.625	1.021	3.751	1.637	1.028
	2 × 2	3.856	1.663	1.032	3.856	1.663	1.032
	4 × 2				3.887	1.671	1.033
	4 × 4	3.887	1.671	1.033			
Coull method		3.981	1.741	1.118	3.981	1.741	1.118
Beam theory		1.000	1.000	1.000	1.000	1.000	1.000

Table 18.10 The bottom stress  $\sigma_y/\sigma_b$  ( $\sigma_b = \frac{PH}{I}b$ ) of a tube structure with rectangular section subjected to horizontal concentrated load

Position		Mid-point A			Corner point B		
$H/b$		2	4	10	2	4	10
TB-12	1 × 1	0.4011	0.7638	0.9352	1.357	1.135	1.013
	2 × 2	0.5541	0.7813	0.9352	1.658	1.274	1.013
	4 × 4	0.5651	0.7835	0.9216	1.930	1.406	1.111
TB-13	1 × 1	0.3173	0.6724	0.9013	1.410	1.197	1.058
	2 × 1	0.5531	0.7681	0.9236	1.701	1.311	1.081
	2 × 2	0.5643	0.7747	0.9081	1.724	1.352	1.115
	4 × 2	0.5630	0.7794	0.9145	1.976	1.445	1.130
Energy method		0.576	0.787	0.915	1.874	1.438	1.175
Coull method		0.5380	0.7680	0.9070	1.577	1.290	1.116
Beam theory		1.0000	1.0000	1.0000	1.000	1.000	1.000

displacement values of Coull method<sup>[16]</sup> given in Table 18.9 are obtained from the force method, so they are larger than the practical displacement values of the structure. Furthermore, with the increase of  $H/b$ , the difference of the tip displacements between numerical result and beam theory will reduce gradually. Results of the vertical stress  $\sigma_y$  at the bottom of the tube structure are listed in Table 18.10. It can be seen that, the stress at the mid-point  $A$  of the edge is smaller than the stress at the corner point  $B$ , which is the so-called “shear lag”. With the increase of  $H/b$ , the shear lag effect will weaken. The stress convergence of the spline element is also very good, and is similar to that of the energy method<sup>[18]</sup>.

**Example 18.8** The internal forces and displacements of a tube structure with a polygonal section subjected to horizontal load (Fig. 18.11(a),(c)).

Geometric parameters:  $b/c = 1, H/b = 2, 4, 10, h = \text{constant}$ ; Physical parameters:  $E = \text{constant}, \mu = 0.3$ . The tube structure with a polygonal section is analyzed by the element TB-13. Numerical solutions of the displacements and stresses are listed in Tables 18.11 and 18.12, respectively, in which the mesh is used for 1/4 of the structure. Satisfactory solutions can be obtained only by a few elements. It can be seen that, the influence of the shear lag effect of the polygonal section tube structure is less than that of the rectangular section tube structure.

**Table 18.11** The tip displacement  $u/u_b \left( u_b = \frac{PH^3}{3EI} \right)$  of a tube structure with polygonal section

$H/b$		2	4	10
Mesh	3 × 1	3.142	1.469	1.000
	6 × 1	3.182	1.480	1.001
	6 × 2	3.182	1.480	1.001
	9 × 2	3.190	1.482	1.002
Beam theory		1.000	1.000	1.000

**Table 18.12** The bottom stress  $\sigma_y/\sigma_b \left( \sigma_b = \frac{PH}{I} b \right)$  of a tube structure with polygonal section

Position		Mid-point $A$			Corner point $B$		
$H/b$		2	4	10	2	4	10
Mesh	3 × 1	0.660	0.855	1.010	1.153	1.062	1.012
	6 × 1	0.761	0.892	0.974	1.313	1.114	1.022
	9 × 1	0.773	0.899	0.975	1.360	1.125	1.023
	6 × 2	0.768	0.880	0.961	1.354	1.156	1.039
	9 × 2	0.771	0.887	0.963	1.426	1.179	1.042
Energy method		0.793	0.897	0.959	1.317	1.159	1.063
Beam theory		1.000	1.000	1.000	1.000	1.000	1.000

(Continued)

Position		Corner point $C$		
$H/b$		2	4	10
Mesh	$3 \times 1$	0.502	0.508	0.505
	$6 \times 1$	0.624	0.544	0.510
	$9 \times 1$	0.643	0.551	0.511
	$6 \times 2$	0.646	0.562	0.515
	$9 \times 2$	0.656	0.571	0.518
Energy method		0.651	0.575	0.530
Beam theory		0.500	0.500	0.500

## References

- [1] De Boor C (1978) A practical guide to splines. Springer Verlag, New York
- [2] Schumaker LL (1981) Spline function: basic theory. John Wiley and Sons, New York
- [3] Schultz MH (1973) Spline analysis. Prentic-Hall, Englewood Cliff, New Jersey
- [4] Prenter PM (1975) Splines and variational methods. John Wiley and Sons, New York
- [5] Yuan S (1982) Finite element analysis of shell of revolution using cubic B spline. In: Proceeding of International Conference on FEM. China, Shanghai, pp 837 – 840
- [6] Yuan S (1986) Quadratic spline thick/thin plate triangular hybrid elements. In: Proceeding International Conference on Computational Mechanics. Tokyo, pp 1111 – 1116
- [7] Fan Z (1988) Applications of spline elements and sub-region mixed elements in structural engineering [Doctoral Dissertation]. Tsinghua University, Beijing (in Chinese)
- [8] Fan Z, Long YQ (1991) Linear analysis of tall buildings using spline element. Engineering Structure, 13: 27 – 33
- [9] Fan Z, Long YQ (1990) Large deflection and stability analysis by geometrically nonlinear spline element. In: Proceeding of International Conference on Numerical Methods in Engineering, Theory & Applications (Vol. 1). Swansea, UK, pp 414 – 422
- [10] Yuan S (1984) Spline elements in stress analysis [Doctoral Dissertation]. Tsinghua University, Beijing
- [11] Cheung YK (1976) Finite strip method in structural analysis. Bergamon Press, Oxford
- [12] Girijavallaham CV (1969) Analysis of shear wall with opening. Journal of ASCE, STR 10: 2093 – 2102
- [13] Chan HC, Cheung YK (1979) Analysis of shear walls using higher order finite element. Building & Environment, 14: 217 – 244
- [14] Fan Z, Long YQ (1989) Spline thick/thin shell element. In: Proceeding of 2nd East Asia-Pacific Conference on Structural Engineering & Construction. Thailand, Chiang Mai, pp1195 – 1200

## **Advanced Finite Element Method in Structural Engineering**

- [15] Coull A, Subedi NK (1975) Hull-core structures subjected to bending and torsion. In: Proceedings of 9th Congress of International Association for Bridge and Structural Engineering, Preliminary Report, May
- [16] Coull A, Bose B (1975) Simplified analysis of framed-tube structures. Journal of the Structural Division, ASCE, 101(11): 2223 – 2240
- [17] Coull A, Bose B (1976) Torsion of framed-tube structures. Journal of the Structural Division, ASCE 102(12): 2366 – 2370
- [18] Long YQ, Xin KG (1985) Analysis of framed-tube structures of polygonal section by energy method. Journal of Building Structures 6(3): 10 – 16 (in Chinese)